Applied Catalysis B: Environmental 180 (2016) 246–254

Contents lists available at ScienceDirect

Applied Catalysis B: Environmental

journal homepage: www.elsevier.com/locate/apcatb

"Nanowire catalysts for ultra-deep hydro-desulfurization and aromatic hydrogenation"

M. Gupta[a,b,1], J. He[a], T. Nguyen[b], F. Petzold[b], D. Fonseca[a], J.B. Jasinski[b], M.K. Sunkara[a,b,*]

[a] Advanced Energy Materials, LLC, USA
[b] Conn Center for Renewable Energy Research, University of Louisville, Louisville, KY 40292, USA

ARTICLE INFO

Article history:
Received 5 November 2014
Received in revised form 5 May 2015
Accepted 16 June 2015
Available online 20 June 2015

Keywords:
ZnO
Nanowire
Diesel
Gasoline
Kerosene
Desulfurization
Reactive adsorption
Aromatic hydrogenation

ABSTRACT

Here, we report high performance catalysts designed using nanowire supports. Specifically, nickel clusters supported on Zinc Oxide (ZnO) nanowires and γ-alumina found to be highly active for ultra-deep desulfurization and aromatic hydrogenation of diesel. They were also found to be highly active for ultra-deep desulfurization of gasoline and kerosene. The catalysts reduced sulfur from diesel, gasoline, and kerosene fuels containing sulfur as high as approximately 200 ppm to less than 1 ppm with sustained activity over testing periods of 100–150 h. The feed contained some of the most difficult to remove sulfur compounds such as 4-methyldibenzothiophene (MDBT), 4,6-dimethyldibenzothiophene (DMDBT). In addition to activity towards ultra-deep desulfurization, these catalysts have shown to be active towards saturate/hydrogenate aromatics in diesel at moderate reaction conditions (30 bar, 290 °C, and LHSV 2.2 h^{-1}). The active catalytic site was determined to be a super Ni rich Ni_xZn_y phase which seemed to remain essentially sulfur free during the reaction. The regenerated catalyst showed reasonable activity toward desulfurization of gasoline.

1. Introduction

Reduction of sulfur in diesel fuel is important for the environment as well as for the performance of catalytic converter in an automobile. Sulfur compounds in the fuels contribute to emissions of SO_2 and sulfate particulate matter. Sulfur in transportation fuels degrades the catalytic converter resulting in increased NO_x and SO_x emissions which increase the potential for causing acid rain. Sulfur must be removed in any catalytic process because it poisons/deactivates the catalyst [1], which otherwise require frequent regeneration or replacement. Likewise, the performance of other catalytic devices such as fuel cells is also extremely sensitive to the presence of sulfur [2].

As of September 2007, all on-highway diesel fuel (ultra-low-sulfur diesel (ULSD)) sold at gas stations in the United States contains less than 15 ppm of sulfur. The demand for ULSD has increased significantly in the last few years [3] because of continual reduction in sulfur limits in transportation fuels. As far as the gasoline is concerned, the Environmental Protection Agency (EPA) proposed a new regulation recently that would reduce its current sulfur content from 30 ppm to 10 ppm by 2017 [4] and much stricter limits are anticipated in future. Therefore, refiners in the United States and Europe have installed numerous new middle distillate hydrotreaters or revamped existing facilities. Governments in developing countries such as India, Mexico, and China are also imposing low sulfur regulations which has increased the demand for ultra-deep desulfurization catalysts around the world [5].

Diesel and gasoline fuels contain a variety of heterocyclic sulfur compounds at few tens of ppm level which are difficult to remove using traditional hydro-sulfurization catalyst used today. For example, many catalysts undergo steric hindrance effects during adsorption with species such as 4-substituted and 4,6-disubstituted dibenzothiophenes. The refractory nature of b-DBTs comes from the steric hindrance around the sulfur atom [3,6]. The removal of these latter compounds presents a significant challenge to the industry [7–10]. The conventional hydro-desulfurization (HDS) process utilizes alumina- and silica-supported cobalt or nickel molybdenum catalyst and operate at 350–390 °C, and pressures between 60 and 90 bars [5]. Currently, for ultra-low sulfur diesel (ULSD) production, hydrotreating catalysts include nickel–molybdenum–sulfur (Ni–Mo–S) or cobalt–molybdenum–sulfur (Co–Mo–S) supported on γ-alumina

* Corresponding author at: Conn Center for Renewable Energy Research, University of Louisville, Louisville, KY 40292, USA.
E-mail address: mahendra@louisville.edu (M.K. Sunkara).
[1] Present address: Chemical & Biomolecular Engineering-MS 362, Rice University, 6100 Main St. Houston, TX 77005-1827, USA.

http://dx.doi.org/10.1016/j.apcatb.2015.06.029
0926-3373/

(Al_2O_3) [3]. However, the above catalysts suffer from low activity for heterocyclic compounds present below 50 ppm and require higher temperature and pressure and/or low space velocities to bring sulfur down below 15 ppm [11,12]. At higher temperatures, there are some inherent issues that reduce the catalyst activity, and they include carbon deposition on catalyst surface and change of catalyst surface itself (re-organization of surface) [12,13]. Hence, there is a crucial need to design high activity catalysts for ultra-deep desulfurization at moderate process conditions. Moreover, the presence of sulfur even at few ppm level can pose significant problems with hydrogen production via diesel reforming for fuel cell applications [14].

Aromatic hydrogenation is also critical for the improvement of fuel quality. Reduction in aromatics improves cetane number thus improves the fuel quality. High aromatic content in diesel results in low cetane number and therefore more NO_x emissions and particulates from diesel and un-combusted hydrocarbon emissions [15]. Hence, it is highly critical to reduce aromatics level in fuel to make it environmentally friendly as well as better fuel quality. For example, Cooper et al. [15] found that when the aromatic content was 37%, the cetane number was 37 for a diesel fuel. The cetane number increased to 48 when aromatic content in diesel was decreased to 20%. Aromatics affect the formation of particulate and polycyclic aromatic hydrocarbons (PAH) emission. A high aromatic content results in a high flame temperature and a low cetane number, which increases NO_x emissions [15]. Also, because aromatics are considered carcinogens, they are regulated to no more than 35% by volume (or 20% by wt) for ULSD. Therefore, a reduction in aromatics is good for both fuel quality and the environment.

Different feed-stocks contain different amounts of aromatics. For example, straight run gas oils usually contain 25–30% total aromatics, whereas cracked distillates – e.g., light cycle oil (LCO) or coker gas oil (CGO) contain 50–75% total aromatics [3]. The industry uses a two-step process: (1) a partial hydrogenation of aromatics on conventional $NiMo/Al_2O_3$ or $CoMo/Al_2O_3$ sulfide catalysts, and then (2) deep hydrogenation on supported noble metal (Pt or Pd; Pd–Pt) catalysts with improved sulfur tolerance [15,16]. Recently, there has been some progress towards one-stage processes [17]. The challenge with catalyst design is that hydrogenation of aromatics takes place during the deep desulfurization of diesel [18]. Therefore, the catalysts need to be highly active towards hydrogenation in the presence of heterocyclic sulfur compounds.

Here, we show the feasibility of using nickel nanoparticles supported on zinc oxide nanowire surfaces as catalysts. Nickel can catalyze the hydrogenation reaction as well as the cleaving of cyclic sulfur compounds like thiophenes. The use of ZnO follows that of reactive adsorption concept in which sulfur from Ni clusters transfer to ZnO nanowire support [19–23]. Tawara's group [20] was the first to report the performance of a Ni/ZnO catalyst as an adsorptive HDS catalyst for the kerosene toward kerosene-fed fuel cell applications. Active nickel sites could be maintained until the ZnO nanowire supports get sulfided fully. ConocoPhillips developed a sulfur removal technology for gasoline, based on reactive adsorption [24].

The use of nanowire support has multi-fold advantages for catalyst design. Some of them are highlighted here: (1) the single crystal nature and faceting improves the properties of the supported catalytically-active metals through the resulting nickel cluster morphology; (2) ability to produce well-defined surface facets therefore higher concentration of desired sites [25]; (2) potentially enhance metal-support interactions; (3) nanowire support undergo less sintering than conventional supports [26,27]; and (4) nanoparticle on nanowire morphology presents an easier diffusion pathway for sulfur transfer from supported clusters to underlying support to maintain a high surface concentration of active nickel sites for deep desulfurization activity.

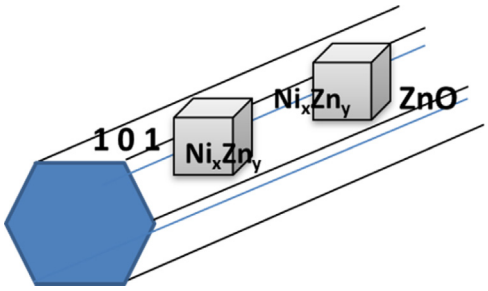

Fig. 1. A schematic showing uniform morphologies for nanoclusters produced on mono-crystalline facets of c-plane oriented ZnO nanowire.

Even though the nanowire supports are predicted to have the above-mentioned advantages, there are no studies for both deep HDS and aromatic hydrogenation using catalysts made from nanowire powders. Here, we report the ultra-deep HDS activity of nickel-rich metal cluster supported on ZnO NWs (Fig. 1). The activity is tested using a variety of fuels and most importantly with diesel that contains one of the most-refractive sulfur compounds, 4,6-Dimethyldibenzothiophene (DMDBT). The nature of active catalyst clusters, uniformity of morphology, morphological stability, and activity of fresh and regenerated catalysts, are of fundamental interest.

2. Experimental

2.1. Catalyst preparation

Several catalyst samples with varying compositions of Ni on ZnO nanowires with and without alumina were prepared. General method used for preparing these catalysts is as follows: ZnO nanowires were produced using an atmospheric plasma jet based reactor described elsewhere [28]. ZnO nanowires were purified to remove ZnO/Zn micro and nanoparticles. A mixture of deionized (DI) water and nanowires was made and sonicated for 10 min and then left to settle for 10 min. The unwanted material quickly settles down in the beaker. The ZnO NW suspensions were decanted into another beaker. Then NH_4OH was added to the suspension to make pH 9.2 (iso-electric point of ZnO NW). Nanowires settle down in a few minutes and then the water was decanted to obtain "pure" ZnO NW. These purified nanowires were then used to prepare catalyst.

A slurry was made by adding DI water to purified ZnO NW and γ-Al_2O_3. Aqueous solutions of nickel acetate ($NiCOOH{\cdot}2H_2O$) was made by adding DI water and by heating and stirring the solution at 90 °C. The nickel acetate solution was added drop-by-drop to the slurry while the mixture being stirred. The pH was maintained around 9.0 by adding aqueous solution of NH_4OH. Then, the mixture was dried at 80 °C for 15 h in a furnace and stirred once during drying. Thereafter, the mixture was dried at 150 °C for a few hours and stirred once to obtain a thick paste for extrusion. Thereafter, the paste was extruded and dried at 150 °C for 1 h. Finally, they were calcined at 390 °C for 2–2.5 h. A batch of extrudates used in this work is shown in Fig. 2. The length and diameter of these extrudates were 4–5 mm and 1–1.5 mm, respectively. These extrudates were then used for the hydro-desulfurization and aromatic hydrogenation tests. With the addition of molybdenyl acetylacetonate, the Ni and Mo supported on ZnO NW catalyst was also prepared using the same synthesis method.

2.2. Ultra-deep desulfurization

First, the catalyst was reduced at 430 °C for 3 h with a H_2 flow rate of 0.15 L/min at atmospheric pressure. The hydro-desulfurization reaction was carried out at 30 bar and 290 °C

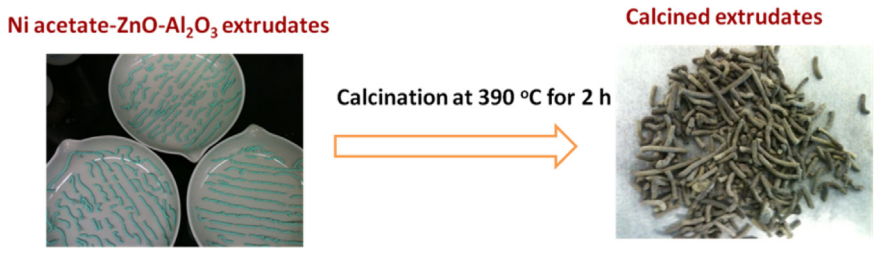

Fig. 2. Extrudates of nickel acetate-ZnO-γ-Al_2O_3 and NiO–ZnO-γ-Al_2O_3.

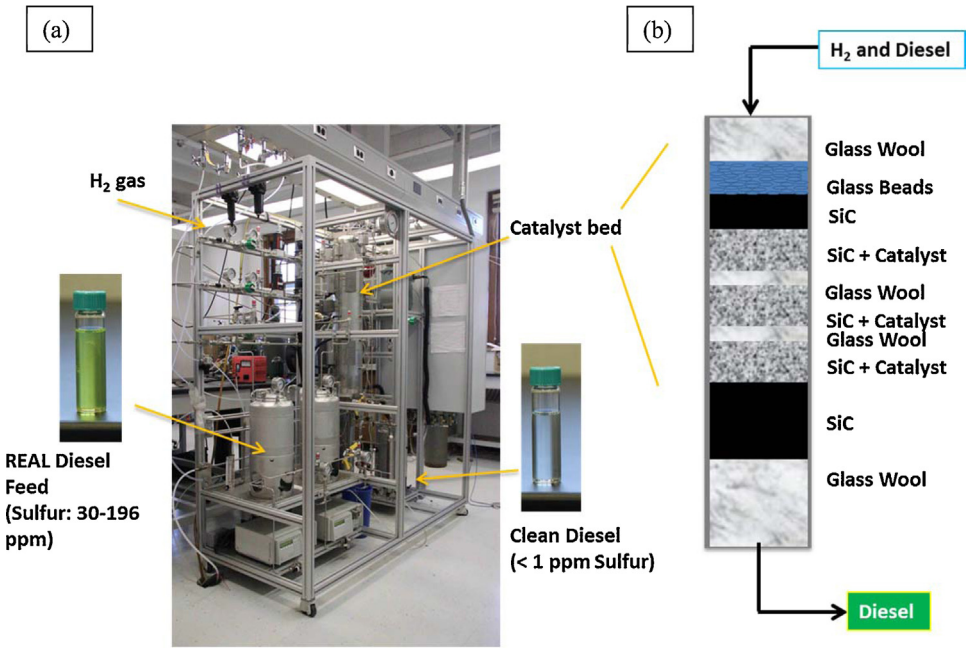

Fig. 3. (a) Photograph of the fixed bed reactor used for desulfurization experiments; (b) Schematic of three zone packing design used in our packed column.

(furnace temperature) with 0.15 L/min H_2 flow. The fixed bed tube (1 inch diameter pipe) was surrounded by a vertical furnace; its temperature was continuously monitored and controlled. The diesel feed rate was 0.36 mL/min. The corresponding liquid hourly space velocity (LHSV) was 2.2 h^{-1}, better than the standard industrial practice for ULSD [3]. A fixed bed reactor (Fig. 3(a)) was used to carry out the reduction, aromatic hydrogenation, and hydrodesulfurization tests.

Catalysts were packed in to the reactor column shown schematically in Fig. 3(b). The extrudates were mixed with SiC to avoid channeling of the fuel and to keep uniform temperature throughout the bed. SiC to Catalyst weight ratio in each layer (Fig. 3(b)) was 3.5. The sulfur species composition and content was varied in our fuel feeds by adding sulfur to ULSD fuel (from a refinery in Kentucky, USA) that originally contained about 9 ppm of sulfur. The sulfur species included most of the difficult to remove thiophenic and benzothiophenic compounds present in actual diesel as shown in Table 1 where C_n is the sum of C_2, C_3, and/or C_4. DF1 contained 9 ppm of sulfur from C_n-DBT and 21 ppm from thiophene; however for DF2, different sulfur compounds were added to increase the final concentration of sulfur to 196 ppm. We used real diesel, gasoline and kerosene feeds. In this work, we used real fuels because they are complex mixtures of several hydrocarbons with varying reactivities. The compositions of fuel samples used in our testing are tabulated in Table 1. The treated samples were collected every few hours during the test. In order to gain insight into the origin of catalytic activity and the composition after desulfurization, both pre-run (fresh) and post-run (spent) catalysts were characterized using BET, scanning electron microscopy (SEM), transmission electron microscopy (TEM), and X-ray diffraction (XRD). Total aromatics were determined using a UV–vis spectrometer. The morphology of the catalysts was studied using a field-emission FEI Nova 600 NanoLab scanning electron microscope (SEM), Bruker Discover D8 powder X-ray diffraction (XRD) system. The identification of the crystal phases was performed using the Powder Diffraction File (PDF) structural database.

An Antek 9000 VS Sulfur analyzer was used to measure sulfur concentration in all the samples. The operation begins with complete high temperature oxidation of the entire sample matrix. The sample is vaporized and combined with oxygen at a temperature of 1250 °C to convert chemically bound sulfur to SO_2. The SO_2 is exposed to ultraviolet radiation of a specific wavelength and the resulting fluorescent emission is completely specific for sulfur and is proportional to the amount of sulfur in the original sample.

3. Results and discussion

3.1. Textural properties of catalysts

Table 2 summarizes the surface area and NiO particle sizes for some of the catalyst samples used in the desulfurization tests. In the catalyst samples A–F, the amount of Ni was varied from 12 to 30 wt%. The BET surface areas were as high as 92.7 m^2/g for 12% Ni catalyst and as low as 8.5 m^2/g for catalyst 17% Ni catalyst

Table 1
Diesel feeds and their sulfur constituents.

Diesel Feed	Sulfur from thiophene (ppm)	Sulfur from 4-Methyldibe-nzothiophene (ppm)	Sulfur from Dibenzothio-phene (DBT) (ppm)	Sulfur from Benzo[b]thio-phene (ppm)	Sulfur from C_n-DBT (ppm)
DF1	21	0	0	0	9
DF2	50	42	42	41	21

Table 2
Catalysts- composition, BET surface area and crystallite size.

Catalysts	Ni (wt%)	ZnO (wt%)	γ-Al_2O_3 (wt%)	BET (m^2/g)	Crystallite Size-NiO (nm)
A	17	83	–	8.5	25.1
B	–	41.6	58.4	123.0	–
C	12	58.7	11.3	92.7	16.0
D	15	58.7	26.3	78.7	10.2
E	21	58.7	20.3	76.9	11.0
F	30	58.7	11.3	46.2	18.9
	Mo (wt%)				
G	12 3	58.7	26.3	59.8	22.0

without γ-Al_2O_3. This indicates that γ-Al_2O_3 helps in increasing the surface of the catalyst because of its higher surface area than nanowires. The metal/oxide can also nucleate on γ-Al_2O_3. The alumina also helps in binding the constituents of the catalyst by imparting mechanical strength to it [3]. The catalyst extrudates without γ-Al_2O_3 became powder after hydro-desulfurization reaction whereas with γ-Al_2O_3 the extrudates retained its shape and size. In general, the crystallite size decreases after addition of γ-Al_2O_3 as shown in Table 2. The catalyst without γ-Al_2O_3 has NiO crystallite size of about 25 nm whereas with γ-Al_2O_3, the size range for NiO crystallites is from 11 to 16 nm. However, addition of Mo increases the crystallite size to 22 nm (Sample G). This is only a preliminary observation and cannot be concluded as a phenomenon. Optimization of active nickel loading is crucial. High content of Ni and low amount of ZnO will provide higher activity initially but will degrade quickly due to low amount of interfacial area between Ni and ZnO. Therefore, in order to obtain long life and high activity, a balance between the compositions of Ni and ZnO is required [20].

3.2. Ultra-deep desulfurization activity testing of catalysts

The ultra-deep desulfurization activities of the catalyst samples from Table 2 were tested using the fixed bed reactor at a temperature of 290 °C, Pressure of 30 bar, and liquid hourly space velocity (LHSV) values ranging from 1 to 2.2 h^{-1}. For diesel and kerosene, the results are shown in Fig. 4(a) and (b). In all cases, the data shows 99% removal of sulfur from feed streams at the moderate process conditions indicating high activity of our nickel supported on ZnO nanowires. Tests were stopped after pre-set times ranging from 100–150 h. In Fig. 4 (a), using our nickel supported on ZnO nanowire catalysts, with a diesel feed (DF2) containing 196 ppm of total sulfur, the sulfur content in the treated diesel was less than 1 ppm. And testing of desulfurization using diesel feed (DF1) containing 30 ppm of sulfur using catalyst containing only ZnO/Al_2O_3 showed sulfur breakthrough in less than 30 h and losing all of the activity in 50 h. The ZnO/Al_2O_3 catalyst showed some activity to reduce sulfur level in the first few hours but the activity was not significant enough to remove sulfur compounds (4,6-dimethyldibenzothiophene and 4-methyldibenzothiophene). The lack of activity with ZnO and γ-Al_2O_3 proves that either Ni or its alloys are required to provide the necessary catalytic activity. As shown in Fig. 4(a), all other catalysts with Ni loading on ZnO NW powder along with γ-Al_2O_3 showed ultra-deep desulfurization to levels less than 1 ppm with steady state activity demonstrated for 100–150 h.

In order to understand the behavior of our catalyst toward fuels other than diesel, we performed a test using sulfur spiked kerosene fuel. Kerosene (carbon range: C_9–C_{16}) represents short chain hydrocarbons compared to diesel (carbon range: C_{10}–C_{19}) and both contain paraffins naphthenes, and aromatics. The composition of jet fuels such as JP-5 and JP-8 is same as kerosene and the only difference is additives present in jet fuels. Therefore, this test is a representative one for various kerosene based fuels such as jet fuels. The data in Fig. 4(b) shows that our catalyst can easily remove sulfur from kerosene. In this test, the catalyst (15% Ni, 58.7% ZnO, 26.3% γ-Al_2O_3) was first reduced at 430 °C for 1.5 h with a H_2 flow rate of 0.15 L/min at atmospheric pressure. The hydrodesulfurization reaction was carried out at 30 bar and 290 °C with 0.15 L/min H_2 flow. The diesel feed rate was 0.32 mL/min. The liquid hourly space velocity (LHSV) was 2.2 h^{-1}. The kerosene grade was K-1 that is used for household purposes that contained originally about 21.7 ppm. An additional amount of 33 ppm of sulfur (thiophene) was added to kerosene to increase total sulfur in the feed. For over 100 h, the sulfur level in treated kerosene remained below 1 ppm.

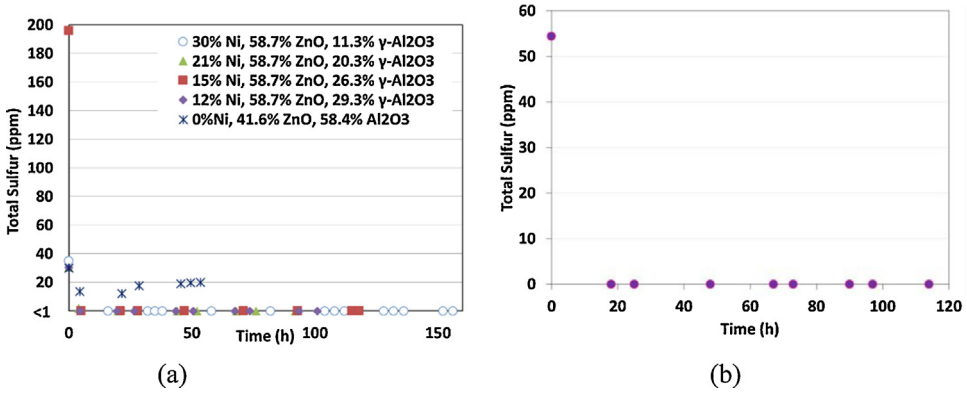

Fig. 4. (a) Sulfur content in diesel at different times-on-stream: Comparison of catalysts using different Ni loading amounts on ZnO NW; (b) Sulfur content in kerosene at different times-on-stream using 15% Ni, 58.7% ZnO, 26.3% γ-Al_2O_3.

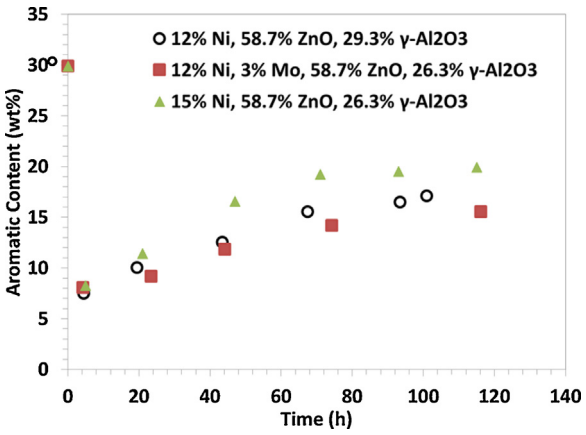

Fig. 5. Total aromatic content in product diesel samples from fixed bed reactor collected over a period of time. Feed contained aromatics close to 30 wt%.

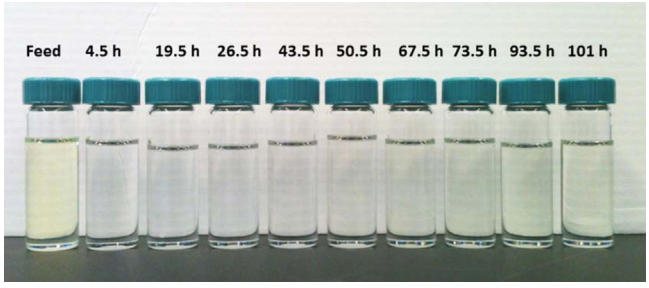

Fig. 6. Color of diesel samples with time.

3.3. Aromatic hydrogenation in diesel

The diesel feeds used in this study contained 29.9 wt% of total aromatics. Fig. 5 shows the performance of three catalysts containing 12%Ni (with and without 3% Mo), and 15% Ni. It is evident from the results that these catalysts are also highly active for aromatic hydrogenation of diesel. The catalysts were able to decrease aromatics from 29.9% to less than 10% in the beginning and reached a steady level of less than 15% in about 100 h. There is no significant change in activity of the catalyst with the addition of Mo. However, the activity decreased when Ni content was increased from 12% to 15% probably due to bigger Ni clusters.

Fig. 6 shows the photographs of treated diesel samples as a function of time. The catalyst was 12% Ni, 58.7% ZnO, 29.3% γ-Al_2O_3. The change in color is probably due to aromatic saturation. Just after few hours, the diesel sample was colorless due to very low amount of aromatics and then started picking up color after 60 hrs and then remained almost the same thereafter, which is consistent with aromatics content in diesel (Fig. 5). Thus, lighter color is indicative of better diesel quality. Another reason could be the generation of color bodies such as polycyclic aromatic molecules after desulfurization of alkyl-dibenzothiophenes. These molecules could be produced by some radicals, the latter were formed when the desulfurized part of alkyl-dibenzothiophenes did not hydrogenate rapidly [29].

3.4. Catalyst regeneration

In order to understand the catalyst regeneration, we first tested our catalyst with gasoline spiked with 880 ppm of sulfur using thiophene and 4,6-DMDBT species. The desulfurization test was carried out at 290 °C, 30 bar, H_2 @ 0.15 L/min, LHSV @ 2.2 h^{-1}. It is evident from Fig. 7 that the catalyst lost most of its activity after 150 h. It is suspected that the catalyst is covered with carbon and/or sulfur

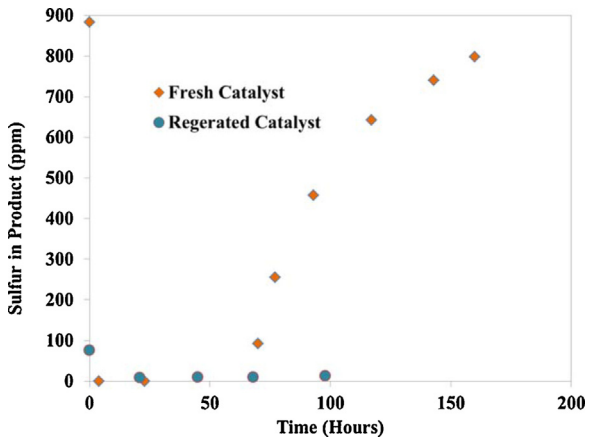

Fig. 7. Sulfur content in gasoline samples at different times-on-stream.

on the surface. The primary product after sulfidation was ZnS in hexagonal (sphalerite) phase. This is highly critical for regeneration of ZnO based adsorbent because ZnS oxidizes directly to ZnO whereas cubic ZnS forms $ZnSO_4$ and $Zn_3O(SO_4)_2$ [30] under mild oxidation conditions.

Regeneration of a deactivated catalyst was done using dry air @ 6 LPM for 1.5 h at 510 °C. The regenerated catalyst showed good activity toward sulfur removal. Fig. 7 shows that sulfur content in the treated gasoline was less than 12 ppm for around 100 h. However, more work is needed to properly regenerate the catalyst to reduce sulfur level down 1 ppm or lower. Regenerability is an important criterion for reducing costs and continuous operation. In the reactive adsorption approach, ultra-deep desulfurization activity will be lost once full sulfidization of the support material occurs; at that point, the active sites can be modified. So, the data suggests that our catalyst could be regenerated to yield a similarly high activity, while retaining both the support morphology (nanowires) and the size and composition of the active metal sites. The data in Fig. 7 shows reasonable success with regeneration of ultra-deep desulfurization activity, nevertheless the performance needs to be improved. Additional experiments using sulfurization of ZnO nanowires using direct reaction with hydrogen disulfide resulted in ZnS phase and re-oxidation also resulted in ZnO nanowire without losing one-dimensional morphology.

3.5. Discussion on activity and mechanism

In order to understand the nature and composition of catalyst site and the sulfur transfer pathway, the spent catalysts are characterized using XRD, XPS and TEM after testing. Fig. 8 shows SEM images for fresh and spent versions of a catalyst containing 15% Ni, 58.7% ZnO, 26.3% γ-Al_2O_3. The diameters and lengths of NWs were 70–150 nm and 250 nm-2 μm, respectively. The spent catalyst was used to desulfurize the DF2 feed containing various sulfur compounds (Table 1) over 110 h. It is clear from the SEM images that the nanowire morphology was retained after reaction. This is highly critical for good activity and selectivity of the catalyst. Fig. 8 shows the XRD patterns for fresh and spent catalysts containing 15% Ni, 58.7% ZnO, 26.3% γ-Al_2O_3. In general, the data shows the presence of NiO and ZnO phases in all the fresh catalysts. There was no shift observed in ZnO peaks. Upon reduction step, NiO clusters reduce to either nickel or nickel rich nickel–zinc compound. The spent catalyst shows ZnS but no NiS phase which supports the reactive adsorption mechanism in which active metal sites are preserved for ultra-deep desulfurization. The absence of NiS phase indicates that the sulfur from sulfided Ni or Ni rich clusters is transferred to underlying ZnO nanowire supports effectively.

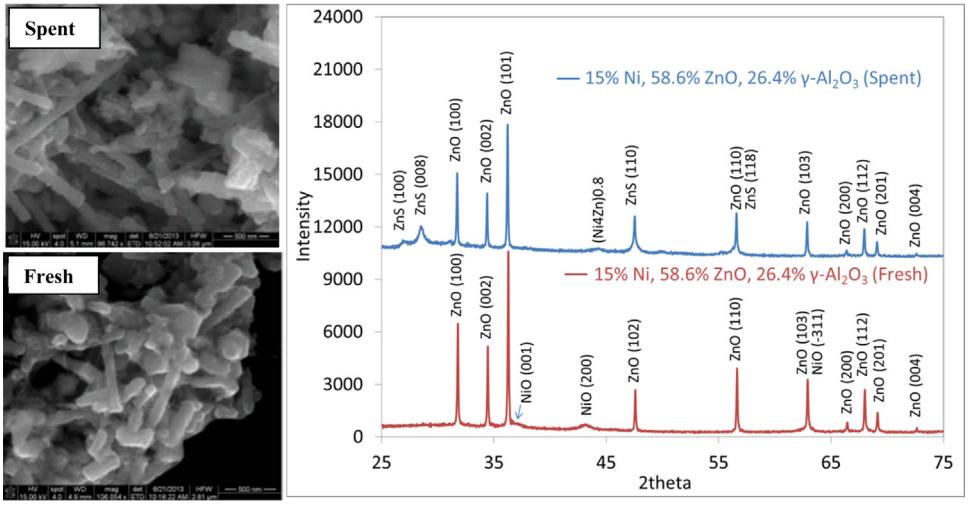

Fig. 8. SEM micrographs and XRD patterns of fresh and spent catalyst 15% Ni, 58.7% ZnO, 26.3% γ-Al_2O_3.

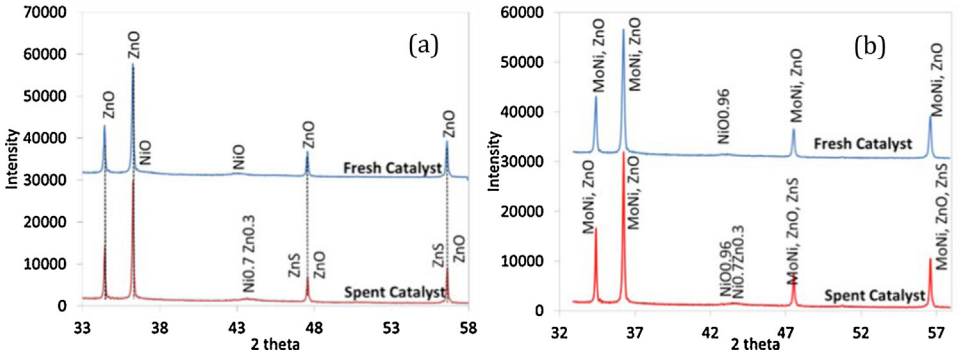

Fig. 9. XRD patterns for fresh and spent catalysts with compositions (a) 12% Ni, 58.7% ZnO, 29.3% γ-Al_2O_3; and (b) 12% Ni, 3% Mo, 58.7% ZnO, 26.3% γ-Al_2O_3.

Fig. 9(a) shows the XRD patterns for fresh and spent catalysts containing 12% Ni, 58.7% ZnO, 29.3% γ-Al_2O_3. The same characteristics were observed as 15% Ni discussed before. It is important to note that, although 15% catalyst and 12% Ni catalyst faced very different amounts of sulfur in the feeds, still there is no significant difference in their XRD features except for nickel-zinc alloy. In the present case, it is $Ni_{0.7}Zn_{0.3}$, whereas in the earlier one it was $(Ni_4Zn)_{0.8}$, both are rich in nickel. It is highly likely that the nickel rich $Ni_{1-x}Zn_x$ alloy clusters are formed during reduction step. It has been shown earlier that reduction at 430 °C enables the formation of nickel alloy with zinc [22]. Fig. 9(b) shows the XRD patterns for 12% Ni, 3% Mo, 58.7% ZnO, 26.3% γ-Al_2O_3. This catalyst contained MoNi, NiO, and ZnO phases. The spent catalyst had MoNi, NiO, ZnO and ZnS phases. This catalyst also did not show any NiS phase which reaffirms our hypothesis of reactive adsorption mechanism.

Fig. 10(a) and (b) show TEM micrographs of ZnO nanowire decorated with NiO nanoparticles in fresh catalyst and nickel-zinc nanoparticles in spent catalyst, respectively. The crystalline size (from XRD) for NiO nanoparticles in fresh catalyst was 10.4 nm and for spent catalyst nickel-zinc crystallite size was 12.8 nm. This shows that the nanoparticles are not agglomerating/sintering to form bigger particles which usually happen with nanoparticles at these reaction conditions. One of the main problems with NPs is sintering [31]. For example, small nanoparticles of ZnO easily agglomerated which caused a catastrophic decrease in both desulfurization activities and sulfur capacities [31]. The formation of bigger particles would be detrimental for steady activity of the catalyst. This observation shows that nanowire supports have prevented the nanoparticles from sintering. This is one of the major qualities of these nanowire-based catalysts. NW morphology was retained, an important characteristic for their continued and steady activity.

In order to further investigate the sulfur adsorption mechanism, a spent catalyst (12% Ni, 58.7% ZnO, 29.3% γ-Al_2O_3) has been analyzed using high resolution TEM (HRTEM) micrographs and the selected-area electron diffraction (SAED) patterns of Ni and NiO. In Fig. 11, the HRTEM images of the different regions of a spent ZnO NW decorated with nickel nanoparticle (A) show that: (B) the nickel cluster on the NW contains both metallic Ni and NiO; (C) the ZnS was found on the NW with the lattice d-spacings of 3.2 Å and 3.17 Å [32], corresponding to the (0 0 2) and the (1 0 0) planes, respectively, which are consistent with the ZnS phase (JCPDS Card No. 80-0007); (D) some unreacted ZnO was present in the core area of the NW with a fringe spacing of 5.27 Å, corresponding to the separation between the (0001) planes [33]. The SAED pattern in Fig. 12(A) was recorded from the nickel cluster presented in Fig. 11(B). In Fig. 12(B), the average radial distribution of ring intensities of this electron diffraction pattern was plotted versus 1/d-spacing, and compared to the Powder Diffraction Files (PDF) of metallic Ni (blue line) and NiO (red line); and it reveals the multiple diffraction rings fit very well to both metallic Ni and NiO structure. Therefore, this HRTEM study also strongly supports the findings from XRD that there is ZnS, not NiS phase in spent catalysts.

The XPS spectra of the spent catalyst 12% Ni, 58.7% ZnO, 29.3% γ-Al_2O_3 were collected and presented in Fig. 13. All the spectra were

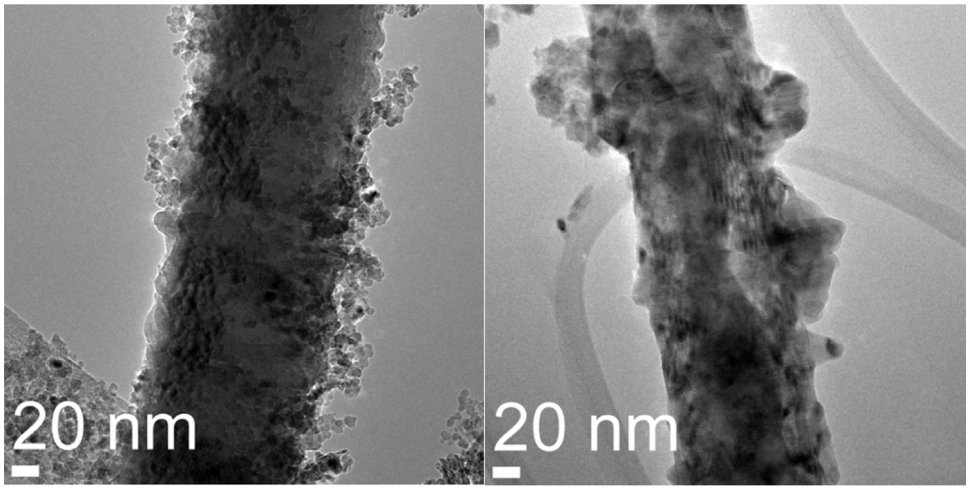

Fig. 10. TEM micrographs of 15% Ni, 58.7% ZnO, 26.3% γ-Al_2O_3 (a) fresh catalyst; (b) spent catalyst. Images do not show the same nanowire but different ones from the same sample.

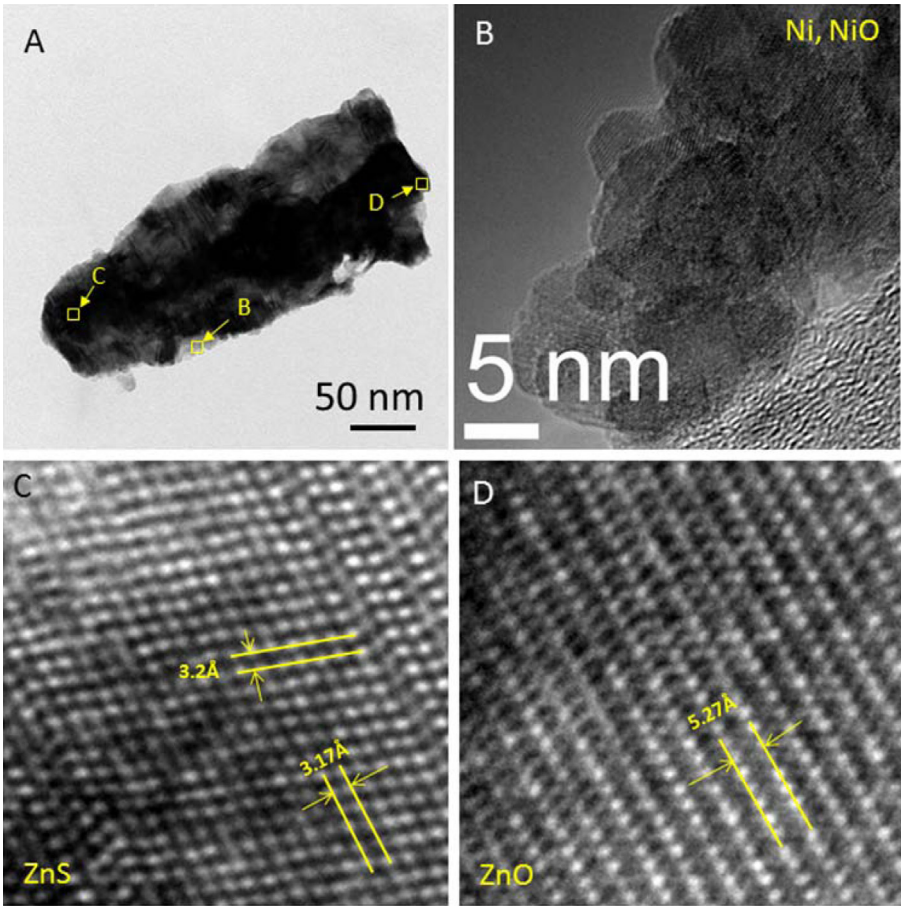

Fig. 11. TEM micrographs of spent catalyst (12% Ni, 58.7% ZnO, 29.3% γ-Al_2O_3): (A) Low-magnification bright filed TEM micrograph; (B) HRTEM image of the selected area in catalyst (A): showing the Ni and NiO cluster; (C) HRTEM image of the selected area in catalyst (A): showing the tail area of the catalyst; (D) HRTEM image of the selected area in catalyst (A): showing the center area of ZnO NW.

decomposed by fitting using Origin Pro. 9.0, in which the black lines represent the experimental data, the red lines are the envelopes of decomposed features and the other lines are the Gaussian components peaks. Fig. 13(A) shows a broad peak assigned to sulfur 2p. The O 1s spectrum is shown in Fig. 13(B) with a binding energy of 531.69 eV, which indicates the oxygen present as metal oxides. In this case, the oxygen is from both NiO and ZnO. In Fig. 13(C), the two main peaks in the XPS spectra of the spent catalyst sample are assigned to the spin-splitting Ni $2p_{3/2}$ and Ni $2p_{1/2}$ and the two broad peaks to the envelopes of their corresponding satellite lines

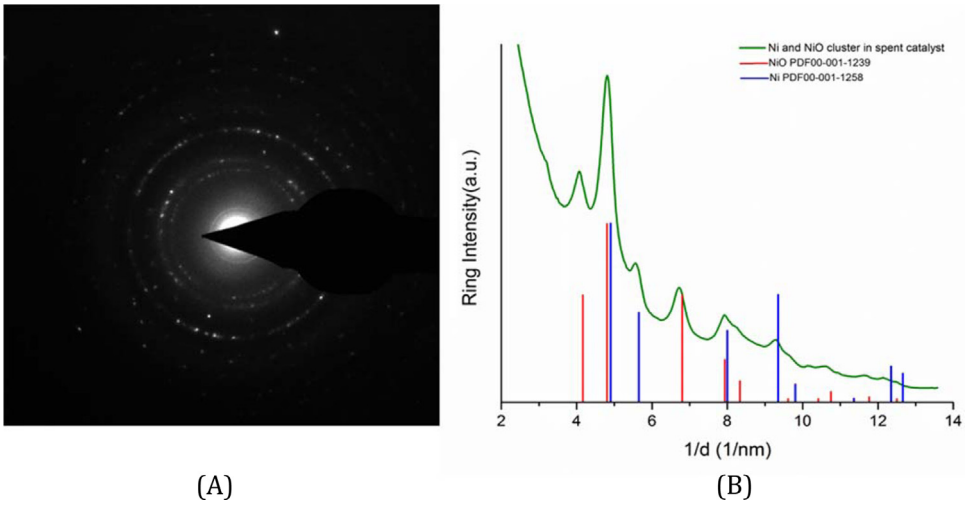

Fig. 12. (A): SAED pattern of Ni cluster of the spent catalyst; (B): Comparison of the electron diffraction patterns plotted as ring intensity versus D-spacing.

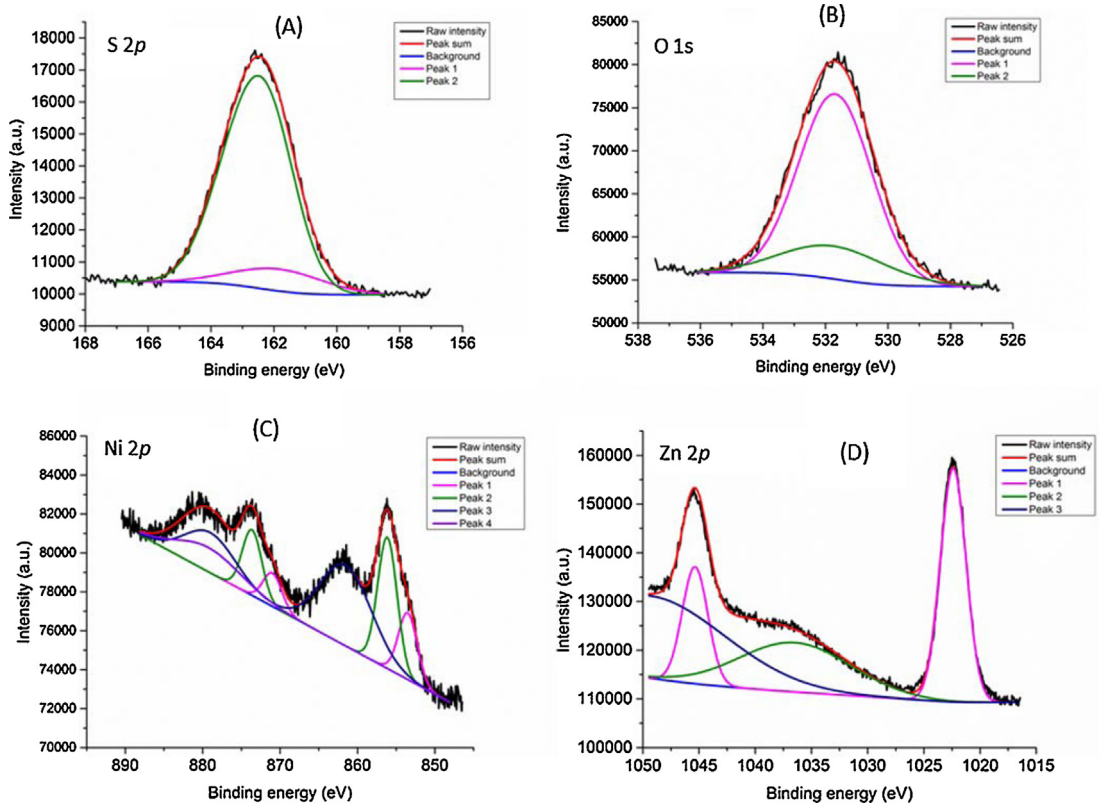

Fig. 13. XPS spectra of spent catalyst 12% Ni, 58.7% ZnO, 29.3% γ-Al_2O_3: (A) S 2p (B) O 1s (C) Ni 2p (D) Zn 2p.

[34]. With a binding energy of 853.50 eV, the nickel species in the spent catalyst can be assigned to Ni^{2+} and Ni in NiO, which are in a good agreement with the observation from the HRTEM study. The Zn 2p spectrum is shown in Fig. 13(D), from the two peaks positions in the spectrum, we could find that the binding energy of Zn $2p_{3/2}$ is at 1022.36 eV in the spent catalyst sample. Many previous literature [35–37] have reported the measured binding energy of ZnO was at 1021.75–1022.5 eV and the ZnS at 1022–1022.6 eV. In this spent catalyst, the peak positions of Zn $2p_{3/2}$ and Zn $2p_{1/2}$ confirm the Zn enrichment in the ZnS compound and the unreacted ZnO NW.

Therefore, it is evident from the XRD, TEM and XPS data that sulfur is associated with Zn not with Ni. This indicates that the transfer of sulfur from the Ni site to ZnO is very efficient, a key to the high activity of the catalyst. Our data also shows the presence of Ni-rich NiZn metal compound clusters which could have facilitated sulfur transfer providing support to arguments posed in Reference [31].

One could potentially hypothesize that desulfurization could result in the formation of H_2S in the gas phase which quickly reacts with ZnO to form ZnS. However, there was no H_2S detected in the exit stream suggesting that this mechanism is not possible. This observation suggests that the likely sulfur transfer mecha-

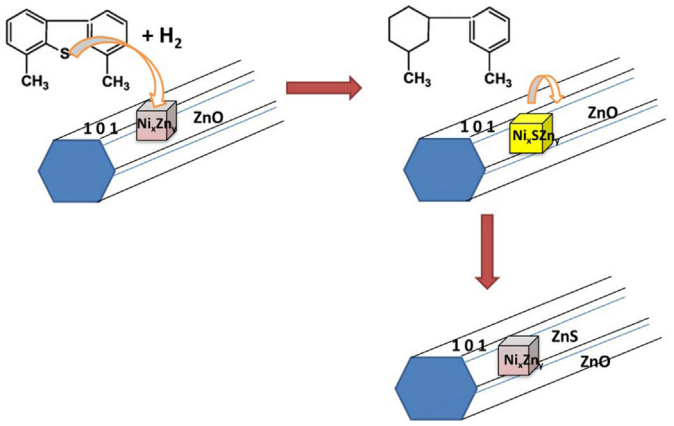

Fig. 14. Proposed reaction mechanism for desulfurization on Ni/ZnO nanowires.

nisms from catalyst site involves solid state pathway, i.e., interface between Ni_xS Zn_y and ZnO.

Fig. 14 shows first the hydrogenation of 4,6-DMDBT. This path is more probable than direct desulfurization (DDS) because sterically hindered C-S bond is easier to break when one of the aromatic rings is first hydrogenated. This step makes sulfur atom more accessible to the active site. Then sulfur is then removed via hydrogenolysis of the C-S bond on the Ni_xZn_y site. This accelerated pre-hydrogenation activity is critical in removing highly refractive sulfur compounds such as 4,6-DMDBT [8,38]. Fresh metal sites provide the suitable environment for the hydrogenation to occur first. The sulfur can directly transfer (solid state diffusion) from Ni_xSZn_y to ZnO. In this mechanism, the NW morphology provides for easier sulfurization and sulfur transfer from active metal particles.

4. Conclusions

Different catalysts containing 12–30% Ni clusters on ZnO nanowire supports and γ-Al_2O_3 were synthesized, characterized, and tested. The sulfur content in diesel, kerosene, and gasoline was brought down to less than 1 ppm from 30 to 200 ppm (approx.) sulfur in different feeds at moderate reaction conditions (pressure 30 bars and temperature 290 °C) compared to industrial practice (60–90 bars and 350–390 °C). The data showed that our catalysts were highly active towards 4,6-Dimethyldibenzothiophene (DMDBT) and also active towards hydrogenation of aromatics at moderate reaction conditions. The steady state activity of the catalyst was achieved within the first few hours and remained constant for over 100 h (after which, the tests were discontinued). In addition to this, approximately 50% of aromatics were reduced in diesel. The active catalytic site was shown to be comprised of super-Ni-rich Ni_xZn_y phase, which remained essentially sulfur free after desulfurization process.

Funding sources

Kentucky Commercialization Fund (KCF) – KSTC (COMMFUND-1325-RFP-012); DOE (DE-EE0003206) and National Science Foundation, Small Business Innovative Research (SBIR) Phase I (Award# 1248696).

Acknowledgments

The authors gratefully acknowledge the funding from Kentucky Commercialization Fund (KCF) – (COMMFUND-1325-RFP-012and National Science Foundation, Small Business Innovative Research (SBIR) Phase I (Award# 1248696) and Phase II (Award# 1248696).

References

[1] V.C. Srivastava, RSC Adv. 2 (2012) 759–783.
[2] B. Alsolami, J.T. Carneiro, J.A. Moulijn, M. Makkee, Fuel 90 (2011) 3021–3027.
[3] A. Stanislaus, A. Marafi, M.S. Rana, Catal. Today 153 (2010) 1–68.
[4] E.P. Agency, Federal Register 78 (2013).
[5] W.R. Inc, (2012).
[6] C.S. Song, Catal. Today 86 (2003) 211–263.
[7] T.C. Ho, Catal. Today 98 (2004) 3–18.
[8] M. Yumoto, K. Usui, K. Watanabe, K. Idei, H. Yamazaki, Catal. Today 35 (1997) 45–50.
[9] S.A. Ali, S. Ahmed, K.W. Ahmed, M.A. Al-Saleh, Fuel Process. Technol. 98 (2012) 39–44.
[10] Q. Gao, T.N.K. Ofosu, S.G. Ma, V.G. Komvokis, C.T. Williams, K. Segawa, Catal. Today 164 (2011) 538–543.
[11] M.E. Pacheco, V.M.M. Salim, J.C. Pinto, Ind. Eng. Chem. Res. 50 (2011) 5975–5981.
[12] E. Furimsky, F.E. Massoth, Catal. Today 52 (1999) 381–495.
[13] C.H. Bartholomew, Appl. Catal. A-Gen. 212 (2001) 17–60.
[14] D. Shekhawat, D.A. Berry, D.J. Haynes, J.J. Spivey, Fuel 88 (2009) 817–825.
[15] B.H. Cooper, B.B.L. Donnis, Appl. Catal. A-Gen. 137 (1996) 203–223.
[16] Y. Yoshimura, M. Toba, T. Matsui, M. Harada, Y. Ichihashi, K.K. Bando, H. Yasuda, H. Ishihara, Y. Morita, T. Kameoka, Appl. Catal. A-Gen. 322 (2007) 152–171.
[17] S.P.T. David Casey, Lawrence Kraus, John Smegal, Yvonne Lucas, Aris Macris, www.digitalrefining.com/article/1000406 (2011).
[18] Y. Zhao, B.J. Shen, W.C. Zhang, R. Tian, Z.H. Zhang, J. Gao, Fuel 87 (2008) 2343–2346.
[19] I.V. Babich, J.A. Moulijn, Fuel 82 (2003) 607–631.
[20] K. Tawara, T. Nishimura, H. Iwanami, T. Nishimoto, T. Hasuike, Ind. Eng. Chem. Res. 40 (2001) 2367–2370.
[21] J. Zhang, Y. Liu, S. Tian, Y. Chai, C. Liu, J. Nat. Gas Chem. 19 (2010) 327–332.
[22] F.G. Petzold, J. Jasinski, E.L. Clark, J.H. Kim, J. Absher, H. Toufar, M.K. Sunkara, Catal. Today 198 (2012) 219–227.
[23] M. Sharma, R.K., Vyas, K., Singh, Adsorpt. -J. Int Adsorpt. Soc. 19 (2013) 161–188.
[24] World review – North America: USA: ConocoPhillips proprietary S-Zorb, Hydrocarbon Eng. 10 (2005) 43.
[25] P. Christopher, S. Linic, J. Am. Chem. Soc. 130 (2008) 11264–11265.
[26] J.F. Da Costa-Serra, R. Guil-Lopez, A. Chica, Int. J. Hydrog. Energy 35 (2010) 6709–6716.
[27] M. Behl, J. Yeom, Q. Lineberry, P.K. Jain, M.A. Shannon, Nat. Nanotechnol. 7 (2012) 810–815.
[28] V. Kumar, J.H. Kim, C. Pendyala, B. Chernomordik, M.K. Sunkara, J. Phys. Chem. C 112 (2008) 17750–17754.
[29] T. Takatsuka, S. Inoue, Y. Wada, Catal. Today 39 (1997) 69–75.
[30] D. Schultze, U. Steinike, J. Kussin, U. Kretzschmar, Cryst. Res. Technol. 30 (1995) 553–558.
[31] Y. Zhang, Y. Yang, H. Han, M. Yang, L. Wang, Y. Zhang, Z. Jiang, C. Li, Appl. Catal. B Environ. 119–120 (2012) 13–19.
[32] Q. Xiong, G. Chen, J. Acord, X. Liu, J. Zengel, H. Gutierrez, J. Redwing, L. Lew Yan Voon, B. Lassen, P. Eklund, Nano Lett. 4 (2004) 1663–1668.
[33] C. Zhao, A., Chen, X., Ji, Y., Zhu, X., Gui, F., Huang, Z. Tang, Mater. Lett. (2015).
[34] J. Cecilia, A. Infantes-Molina, E. Rodríguez-Castellón, A. Jiménez-López, J. Catal. 263 (2009) 4–15.
[35] J.F. Moulder, J., Chastain, R.C., King, Handbook of X-ray photoelectron spectroscopy: a reference book of standard spectra for identification and interpretation of XPS data, Perkin-Elmer Eden Prairie, MN, 1992.
[36] M. Chen, X. Wang, Y. Yu, Z. Pei, X. Bai, C. Sun, R. Huang, L. Wen, Appl. Surf. Sci. 158 (2000) 134–140.
[37] K. Laajalehto, I. Kartio, P. Nowak, Appl. Surface Sci. 81 (1994) 11–15.
[38] T. Fujikawa, J. Jpn. Pet. Inst 50 (2007) 249–261.